Electronic Supplementary Material (ESI) for Nanoscale.

Photoregulative Phase Change Biomaterials Showing Thermodynamic and Mechanical Stabilities

Lei Zhang,[a] Jingjing Gu,[a] Xiliang Luo,*[a] Zhenyu Tang,[a] Yang Qu,[a] Chenghao Zhang,[a] Han Liu,[a] Jishuai Liu,[a] Congxia Xie and Zhongtao Wu*[a]

[a] *Key Laboratory of Optic-electric Sensing and Analytical Chemistry for Life Science, MOE; Shandong Key Laboratory of Biochemical Analysis; College of Chemistry and Molecular Engineering, Qingdao University of Science and Technology, Qingdao, 266042, China*

1. General remarks

Meterials: the materials used for the preparation of DNA complexes, including DNA (5'-CCTCGCTCTGCTAATCCTGTTA-3', M.W. = 6612.4) purchased from Sangon Biotech (Shanghai) Co. Ltd., dioctyldimethylammonium bromide (DOAB) purchased from TCI (Tokyo Chemical Industry Co., Ltd), were used directly without further purifications. All the solutions were prepared using ultrapure water through a Millipore Milli-Q 185 water purification system (Millipore, USA).

Characterizations of 1 and DNA melts: ^{1}H-NMR and ^{13}C-NMR spectra were recorded on Bruker Avance 500 (500 and 125 MHz, respectively) or Bruker Avance 400 (400 and 100 MHz, respectively) with $CDCl_3$ as solvent. Chemical shifts were determined relative to the residual solvent peaks ($CHCl_3$, δ = 7.26 ppm for ^{1}H NMR, δ = 77.0 ppm for ^{13}C-NMR). The following abbreviations are used to indicate signal multiplicity: s, singlet; d, doublet; t, triplet; m, multiplet; br, broad. Mass spectra were recorded on a Thermo Scientific LTQ Orbitrap XL machine. TGA was carried out using a Netzsch STA 449C thermal analyzer in a nitrogen atmosphere and with a heating/cooling rate of 10 ^{o}C min^{-1}. DSC was performed by a Netzsch DSC204F1 machine with a heating rate of 5 ^{o}C min^{-1}. POM was conducted on a Nikon ECLIPSE LV100NPOL machine with a computational controlled heating plate. SAXS was performed by employing a conventional X-ray source with radiation wavelength of λ = 1.54 Å. The sample holder is a metal plate with a small hole (diameter ≈ 0. 5 cm, thickness ≈ 0. 5 cm), where the X-ray beam passes through and the sample-to-detector distance was 18 cm. The scattering vector q is defined as $q = 4\pi \sin\theta/\lambda$ with 2θ being the scattering angle. Rheology was investigated by a Discovery HR-2 hybrid rheometer (TA instruments-Waters LLC, USA). The viscoelastic properties were determined by an oscillatory measurement from 0.01 to 20 Hz. The UV-Vis absorption spectra were recorded on a Shimadzu UV-2600 UV-Vis spectrophotometer, and all the related studies were carried out on fast scan mode with slit widths of 1.0 nm, using matched quartz cells. Test solutions were 200 μL. All absorption scans were saved as ACS II files and further processed in OriginLab software to produce all graphs shown. The wavelengths of UV and Vis photoirradiations are 365 nm (31.8 mW cm^{-2}) and 520 nm (95.5 mW cm^{-2}), respectively.

2. Synthesis of ammonium surfactant 1

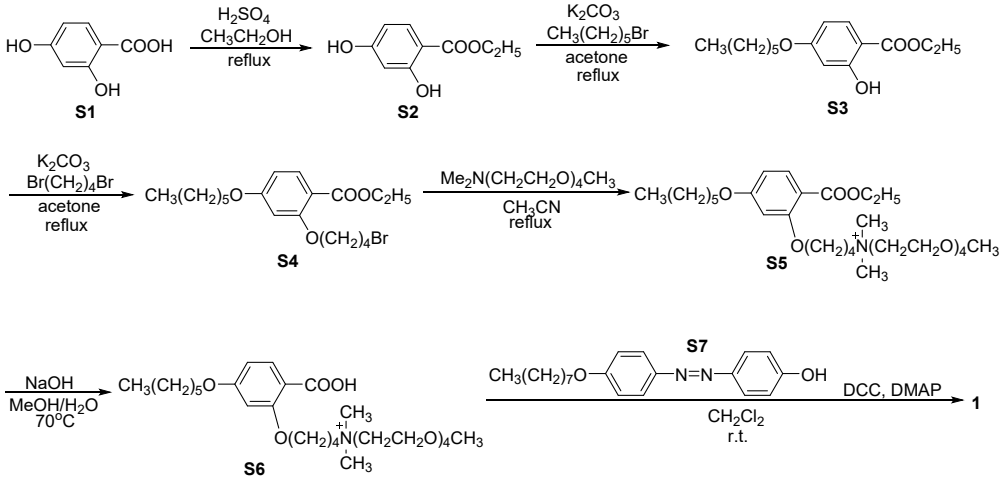

Scheme S1. Synthesis of AZO surfactant **1**.

Ethyl 2,4-dihydroxybenzoate (S2): To a solution of 2,4-dihydroxybenzoic acid **S1** (10 g, 64.88 mmol) in ethanol (50 mL) was added H_2SO_4 (2.0 mL) dropwisely. The resulted mixture was refluxed overnight. The mixture was cooled to room temperature and the pH was adjusted to 5~6 by adding saturated $NaHCO_3$ (aq). The mixture was extracted with Et_2O, and the combined organic layers were dried over Na_2SO_4, concentrated in vacuo. The residue was purified by column chromatography on silica gel (petroleum ether/EtOAc = 8 : 1) to afford **S2** (8.04 g, 68% yield) as colorless oil. ^{1}H NMR spectra coincided with those reported in the literature.[1]

Ethyl 4-(hexyloxy)-2-hydroxybenzoate (S3): To a solution of **S2** (6.0 g, 32.93 mmol) in acetone (40 mL) were added 1-bromohexane (5.55 mL, 39.53 mmol, 1.2eq) and K_2CO_3 (13.66 g, 98.84 mmol, 3eq). The resulted mixture was refluxed for 24 h. After cooling to room temperature, the mixture was concentrated in vacuo and subsequently dissolved in $CHCl_3$. The mixture was filtered and the filtrate was concentrated in vacuo. The residue was purified by column chromatography on silica gel (petroleum ether/EtOAc = 6 : 1) to afford **S3** (6.23 g, 71% yield) as a white crystal. ^{1}H NMR (500 MHz, $CDCl_3$) δ 11.05 (s, 1 H)，7.73 (d, J = 9.5 Hz, 1 H), 6.43-6.41 (m, 2 H)，4.37 (q, J = 7.0 Hz, 2 H)，3.97 (t, J = 6.5 Hz, 2 H)，1.80-1.75 (m, 2 H)，1.46-1.43 (m, 2 H)，1.39 (t, J = 7.0 Hz, 3 H), 1.34-1.33 (m, 4 H)，0.90 (t, J = 6.5 Hz, 3 H); ^{13}C NMR (100 MHz, $CDCl_3$) δ 170.1, 165.1, 163.8, 131.1, 107.8, 105.4, 101.1, 68.3, 60.9, 31.5, 29.0, 25.6, 22.5, 14.2, 14.0; HRMS (ESI) m/z calcd for $C_{15}H_{23}O_4^+$ $[M + H]^+$ 267.1591, found 267.1592.

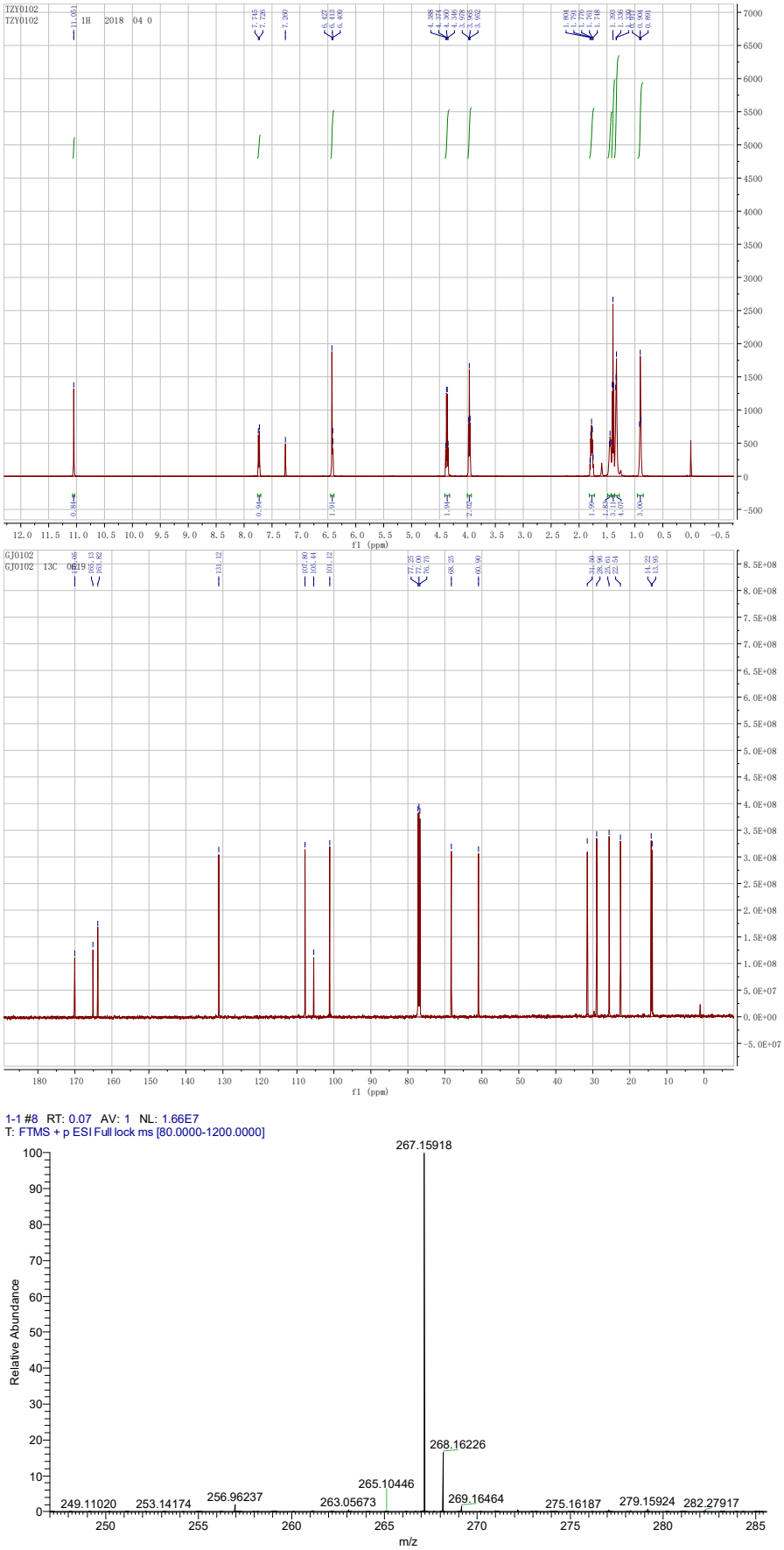

Figure S1. Copies of ^{1}H NMR, ^{13}C NMR and HRMS of **S3**.

Ethyl 2-(4-bromobutoxy)-4-(hexyloxy)benzoate (S4): To a solution of **S3** (5.0 g, 18.77 mmol) in acetone (30 mL) were added 1,4-dibromobutane (2.69 mL, 22.53 mmol, 1.2eq) and K_2CO_3 (3.89 g, 28.15 mmol, 1.5eq). The resulted mixture was refluxed over 24 h. After cooling to room temperature, the mixture was filtered and the filtrate was concentrated in vacuo. The residue was purified by column chromatography on silica gel (petroleum ether/EtOAc = 10 : 1) to afford **S4** (6.78 g, 90% yield) as colorless oil. ^{1}H NMR (400 MHz, $CDCl_3$) δ 7.82 (d, J = 8.4 Hz, 1 H), 6.48-6.43 (m, 2 H), 4.31 (q, J = 7.2 Hz, 2 H), 4.03 (t, J = 6.0 Hz, 2 H), 3.97 (t, J = 6.4 Hz, 2 H), 3.50 (t, J = 6.4 Hz, 2 H), 2.16-2.10 (m, 2 H), 2.02-1.95 (m, 2 H), 1.80-1.73 (m, 2 H), 1.48-1.41 (m, 2 H), 1.37-1.31 (m, 7 H), 0.92-0.88 (t, J = 7.2 Hz, 3 H); ^{13}C NMR (100 MHz, $CDCl_3$): δ 165.8 163.6, 160.4, 133.7, 112.6, 105.2, 100.1 , 68.2, 67.5, 60.3, 33.6, 31.5, 29.3, 29.0, 27.7, 25.6, 22.5, 14.4, 14.0; HRMS (ESI) calcd. $C_{19}H_{30}BrO_4$ $[M + H]^+$ 401.1322, found 401.1326.

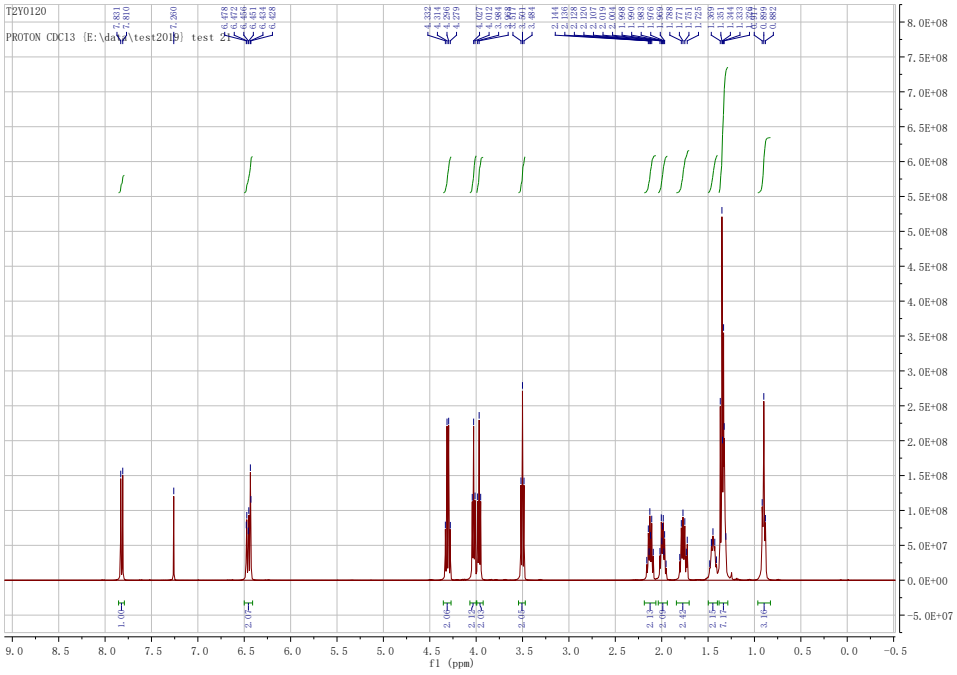

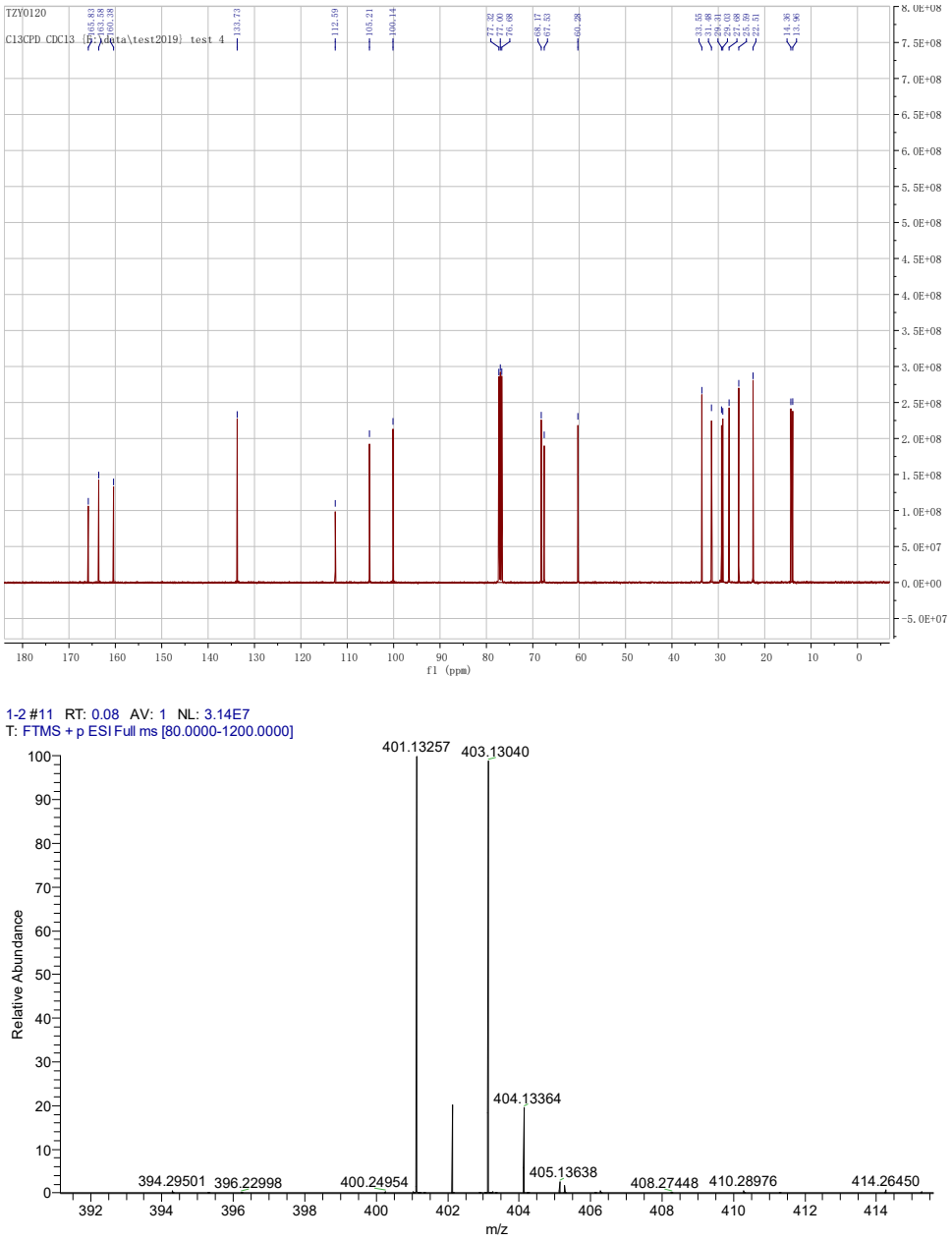

Figure S2. Copies of ^{1}H NMR, ^{13}C NMR and HRMS of **S4**.

***N*-(4-(2-(ethoxycarbonyl)-5-(hexyloxy)phenoxy)butyl)-*N*-methyl-*N*-(2,5,8,11-tetraoxatridecan-13-yl)methyliumaminium (S5):** to solution of **S4** (4.0 g, 9.97 mmol) in CH_3CN (15 mL) was added $Me_2N(CH_2CH_2O)_4CH_3$ (2.11 g, 8.97mmol, 0.9eq). The resulted mixture was refluxed over 24 h. After cooling to room temperature, the mixture was concentrated in vacuo, and the residue was put into next step without further purification.

Note: $Me_2N(CH_2CH_2O)_4CH_3$ was prepared following a reported procedure.[2]

***N*-(4-(2-carboxy-5-(hexyloxy)phenoxy)butyl)-*N*-(λ^3-methyl)-N-methyl-2,5,8,11-**

tetraoxatridecan-13-aminium (S6): to a solution of **S5** obtained from last step in MeOH/H_2O (30 mL, 10:1) was added sodium hydroxide pellets (1.0 g, 25.00 mmol, 2.6 eq). The resulted mixture was refluxed over 12 h. After cooling to room temperature, the mixture was acidified to pH ~2-4 by HCl (conc., 12 M). The mixture was concentrated in vacuo to remove the MeOH and the residue was extracted with $CHCl_3$, and the organic layer was separated, dried and concentrated in vacuo. The residue was put into next step without further purification.

(*E*)-*N*-(4-(5-(hexyloxy)-2-((4-((4-(octyloxy)phenyl)diazenyl)phenoxy)carbonyl)phenoxy)butyl)-*N*,*N*-dimethyl-2,5,8,11-tetraoxatridecan-13-aminium (1): to a solution of residue obtained from last step in dry CH_2Cl_2 (15 mL) were added **S7** (3.25 g, 9.97 mmol, 1.0 eq), EDC (1.90 g, 9.97 mmol, 1.0 eq), HOBt (1.35 g, 9.97 mmol, 1.0 eq) and DIPEA (1.65 mL, 9.97 mmol, 1.0 eq). The resulted mixture was stirred at room temperature over 24 h. The filtrate was concentrated in vacuo and subsequently purified by column chromatography on silica gel (EtOAc/EtOH/H_2O = 3:2:0.5) to afford **1** (1.92 g, 21% yield over 3 steps) as yellow oil. ^{1}H NMR (500 MHz, $CDCl_3$) δ 8.05 (d, J = 9.0 Hz, 1 H), 7.90 (d, J = 9.0 Hz, 2 H), 7.87 (d, J = 9.0 Hz, 2 H), 7.25 (d, J = 9.5 Hz, 2 H), 6.98 (d, J = 9.0 Hz, 2 H), 6.53 (dd, J = 9.0, 2.0 Hz, 1 H), 6.47 (d, J = 2.0 Hz, 1 H), 4.08 (t, J = 5.0 Hz, 2 H), 4.01 (dd, J = 12.0, 6.5 Hz, 4 H), 3.77-3.72 (m, 4 H), 3.652-3.645 (m, 2H), 3.55-3.48 (m, 10 H), 3.45-3.43 (m, 2 H), 3.28 (s, 3 H), 3.17 (s, 6 H), 2.09-2.01 (m, 2 H), 1.92-1.89 (m, 2 H), 1.82-1.75 (m, 4 H), 1.48-1.42 (m, 4 H), 1.35-1.23 (m, 12 H), 0.90-0.85 (m, 6 H); ^{13}C NMR (100 MHz, $CDCl_3$) δ 165.0, 163.2, 161.9, 161.6, 152.5, 150.3, 146.7, 134.4, 124.8 (X 2), 123.7 (X 2), 122.6 (X 2), 114.8 (X 2), 110.0, 106.1, 100.0, 71.8, 70.5, 70.4 (X 2), 70.2, 70.1, 68.5, 68.4, 68.0, 65.5, 64.9, 63.0, 58.9, 51.6 (X 2), 31.8, 31.5, 29.3, 29.22 (X 2), 29.18, 29.0, 26.0, 25.6, 22.7, 22.6, 20.0, 14.1, 14.0; HRMS (ESI) m/z calcd. for $C_{48}H_{74}N_3O_9^+$ $[M - Br]^+$ 836.5420, found 836.5411.

Note: **S7** was prepared following a reported procedure.[2]

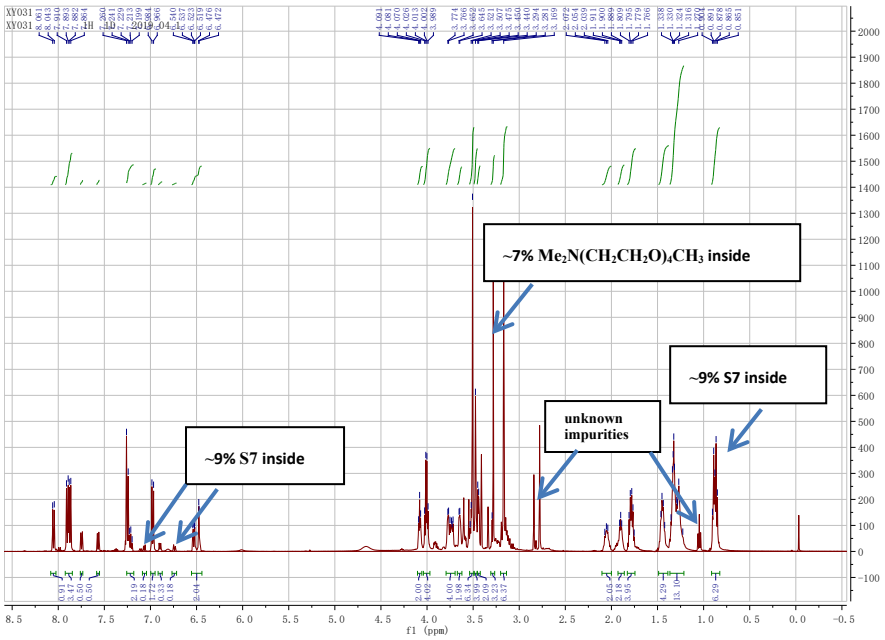

The ^{1}H NMR of **1** gives information on the purity. The m peak at 0.90-0.85 ppm with 6.29 H integration is assigned to two CH_3- groups from -C_6H_{13} and -C_8H_{17} chains of **1**, while, in principle it should be 6 H. In the last three steps, the intermediate compound S4 is the direct starting material to **1**, which is in good purity according to the t peak from the end CH_3- group of -C_6H_{13} of S4 in ^{1}H NMR spectra in Figure S2 (a slight higher integration more than 3 H for this CH_3- group of S4 should originate from the standard integration for 1 H from phenyl group.) Thus, the extra 0.29 H at 0.90-0.85 ppm of **1** ^{1}H NMR spectrum is from the unreacted S7 in the final synthetic step, which means that in molecular concentration ~9% of S7 is still inside the obtained **1**. The peak at 3.28 ppm with (3 + 0.23) H integration is assigned to –OCH_3 group of **1** and the unreacted amine compound from S4-to-S5 step, indicating ~7% molecular concentration of amine in **1**. The peaks at 2.84, 2.78 and 1.05 ppm are from unknown impurities, which were hardly assigned to known functional groups. These unknown impurities were probably introduced from the solvents during the workups. From the region at 8.06-6.47 ppm, four groups of d peak with integration of ~0.18 H at 7.75, 7.57, 7.07 and 6.74 ppm were found, in accordance with ~9% of S7 in **1**. Four groups of d peak with integration of ~0.33 H at 7.75, 7.57, ~7.22 and 6.90 ppm were found, which were assigned to be the *cis*-isomer of **1**, indicating the isomer ratio in about 5:1. Here, the peak at ~7.22 ppm is combined with the two phenyl protons neighboring –OC_8H_{17} and the residual solvent peak at 7.26 ppm. The peaks at 7.75 and 7.57 ppm were the combination of 0.18 H and 0.33 H. An interaction between the phenyl groups from **1** and S7 might be the reason for this coincident combination. The final obtained product **1** was purified by chromatography on silica gel repeatedly over two times, but it is still very hard to remove the residual S7 and $Me_2N(CH_2CH_2O)_4CH_3$ due to the strong molecular interactions from 1) azobenzene groups from S7 and **1**, and 2) PEG chains from $Me_2N(CH_2CH_2O)_4CH_3$ and **1**. In general, the purity of **1** in mass concentration is around 94.8%, if not taking the unknown impurities into account. It is worth noting that these unknown impurities from solvents are normally small molecules, as compared to the molecular weight (917.04 g/mol) of **1**. Therefore, the calculated 94.8% purity would be close to the actual purity.

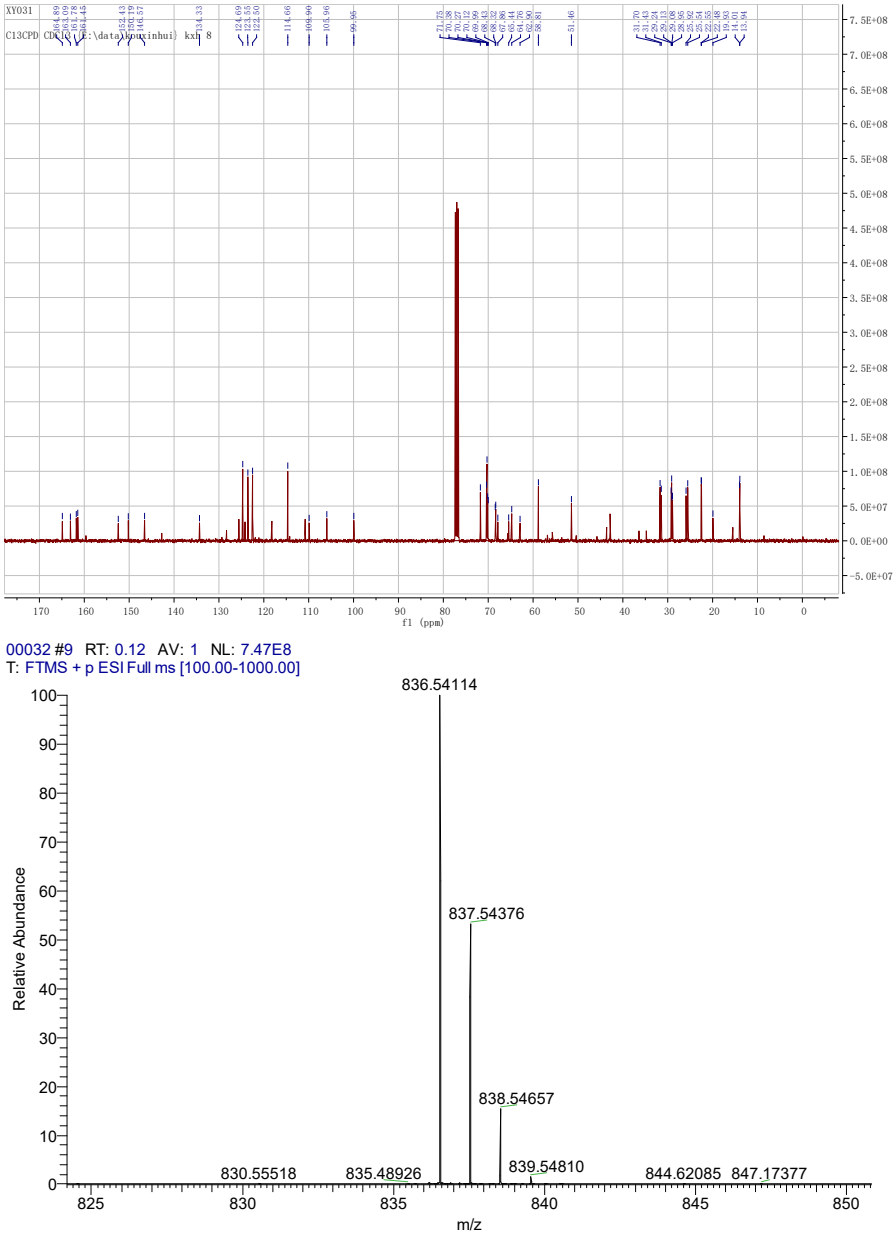

Figure S3. Copies of ^{1}H NMR, ^{13}C NMR and HRMS of **1**.

3. Synthesis of DNA melts

DNA-1 (1:5): the aqueous solution of **1** (23.6 mM, 140 μL) was added into the aqueous DNA (5'-CCTCGCTCTGCTAATCCTGTTA-3') solution (1.5 mM, 20 μL) using a pipette, which led to the precipitate of DNA-**1** complex. The precipitate was purified by centrifugation over three times and lyophilization to afford the needed DNA-**1** (1:5) TLC.

DNA-1-DOAB (1:x:y): DNA-**1**-DOAB (1:x:y) was prepared following a procedure as that of DNA-**1** (1:5), but using **1** (23.6 mM, 112 μL) and DOAB (65 mM, 10.2 μL) for DNA-**1**-DOAB

(1:4:1), **1** (23.6 mM, 84 μL) and DOAB (65 mM, 20.3 μL) for DNA-**1**-DOAB (1:3:2), **1** (23.6 mM, 56 μL) and DOAB (65 mM, 30.5 μL) for DNA-**1**-DOAB (1:2:3), **1** (23.6 mM, 28 μL) and DOAB (65 mM, 40.6 μL) for DNA-**1**-DOAB (1:1:4), respectively.

4. Characterizations of ammonium surfactant 1 and DNA TLCs

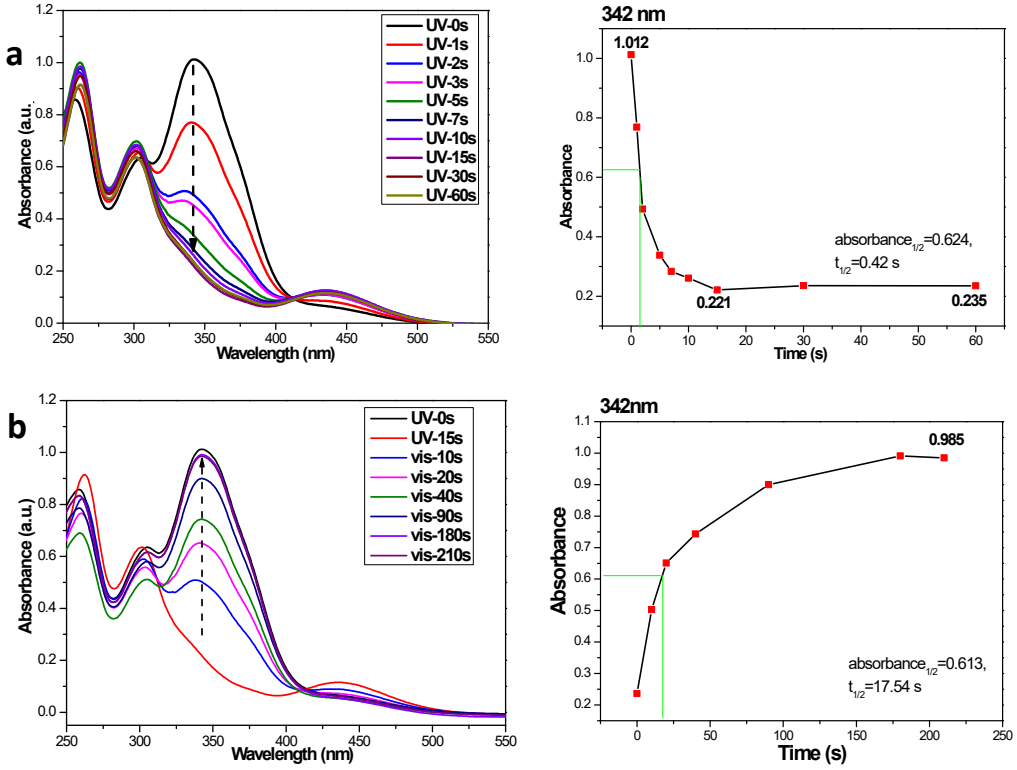

The *trans-cis* isomerization yields of **1** between the most *trans*-rich and the most *cis*-rich states were estimated by following the methods: *cis*-**1**% = $(A_{PSS\text{-}UV} - A_{trans})/(A_{cis} - A_{trans})$ = 97.5% and *trans*-**1**% = $(A_{PSS\text{-}Vis} - A_{cis})/(A_{trans} - A_{cis})$ = 96.6%.[3] **1** undergoes utmost *trans-cis* conversion after ~15 s UV light irradiation, while then gradually reach to the photostationary state with slightly decreasing the ratio of *cis*-**1**. (The ratio decrease of *cis*-**1** after 15 s under continuous UV light irradiation should be caused by the molecular orientation during the *trans-cis* isomerization.[4]) Here, we determine the utmost conversion to *cis*-**1** to be the most *cis*-rich state (A_{cis} = 0.221). Under Vis light irradiation, **1** undergoes utmost *cis-trans* conversion after ~180 s irradiation, and then reach to the photostationary state, with the absorption intensity lower than the initial thermal stationary state. Therefore, we determine the initial thermal stationary state to be the most *trans*-rich state (A_{trans} = 1.012). The $A_{PSS\text{-}UV}$ (0.235) and $A_{PSS\text{-}Vis}$ (0.985) are the absorption values from the final photostationary states under UV and Vis light irradiations at 60 s and 210 s, respectively.

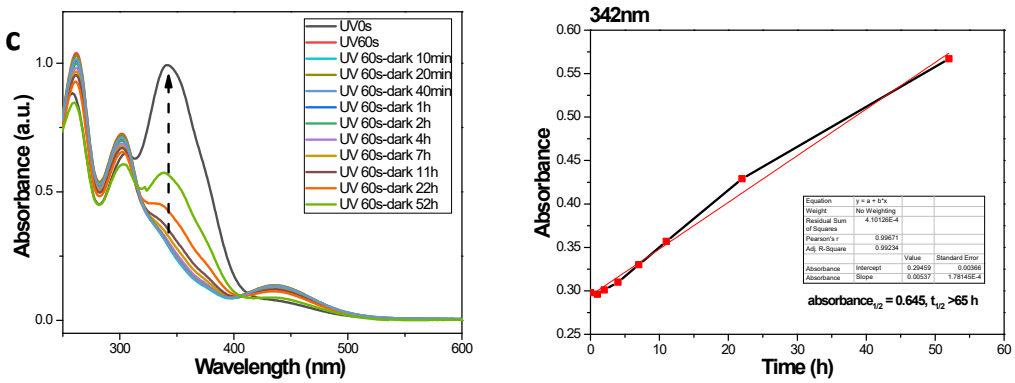

Figure S4. Time-dependent UV-Vis absorption spectral changes of **1** in aqueous solution (60.4 μM) at r.t. under **a**) UV light, **b**) firstly UV light over 15 s and then Vis light and **c**) firstly UV light over 60 s and then in dark. The maximum absorption peak at 342 nm for π-π* absorption is used for drawing the plotted graphs.

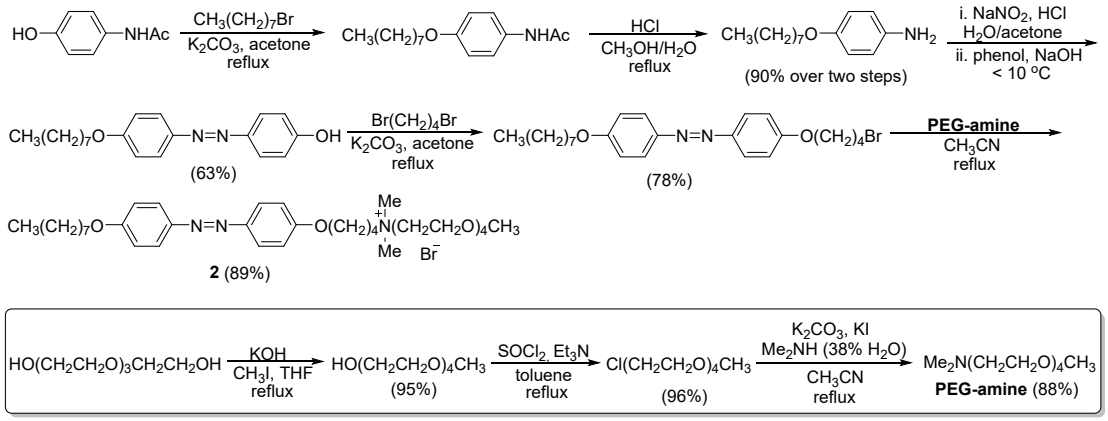

Scheme S2. Synthesis of AZO surfactant **2**. Surfactant **2** was prepared in 39% yield over 5 steps according to our reported synthetic route starting from 4-acetoamidophenol.[2]

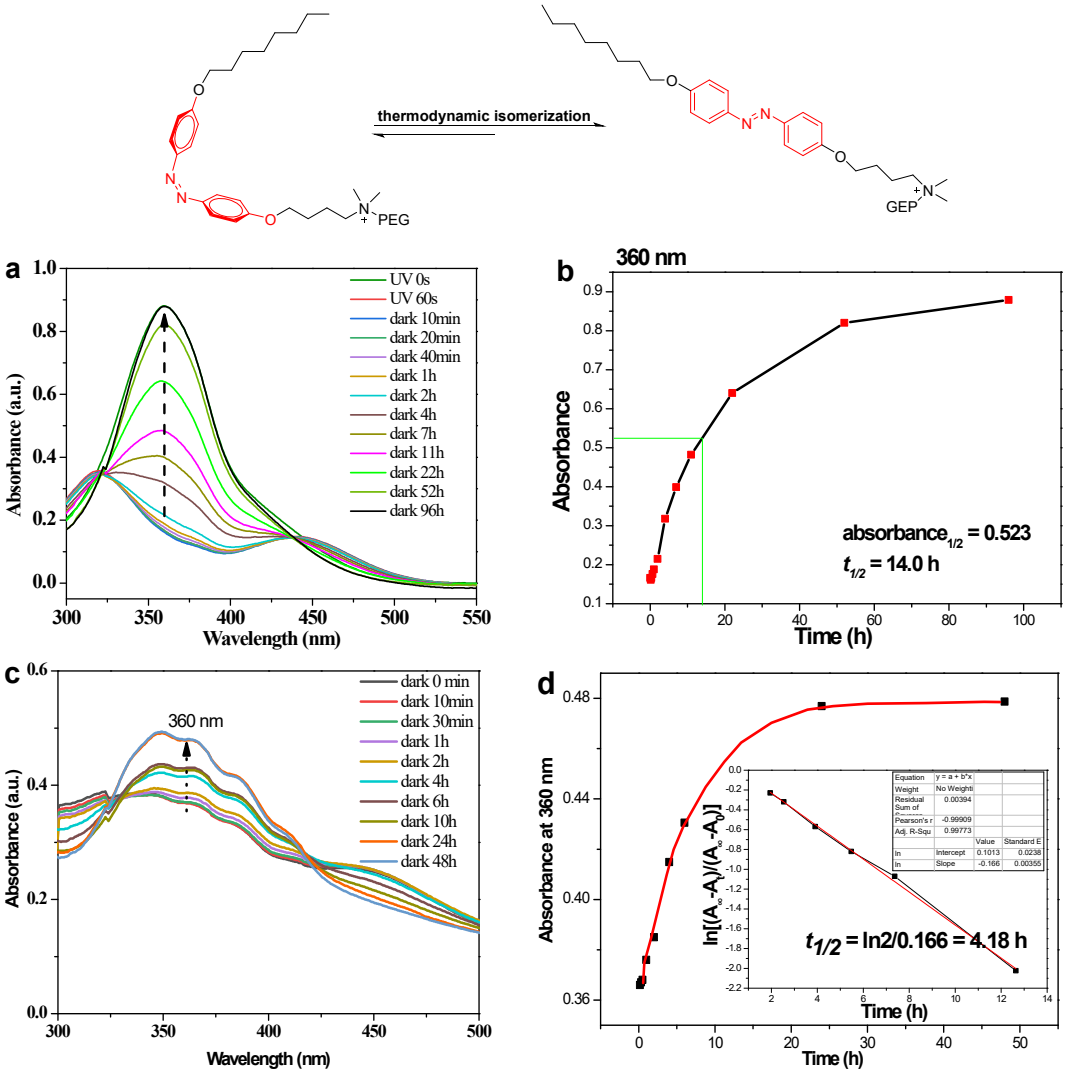

Figure S5. a) Time-dependent UV-Vis absorption spectral changes of **2** in aqueous solution (43.9 μM) at r.t. under firstly UV light over 60 s and then in dark. b) The maximum absorption peak at 360 nm for π-π* absorption of **2** is used for drawing the plotted graph, affording the half-life (14.0 h) for *cis*-**2** in aqueous condition. c) Time-dependent UV-Vis absorption spectral changes of **2** in solid state at r.t. under firstly UV light over 10 min and then in dark. d) The absorption peak at 360 nm for π-π* absorption of *cis*-**2** is used for drawing the plotted graph, affording the half-life (4.18 h) for solid-state *cis*-**2**. Equation of $\ln[(A_\infty-A_t)/(A_\infty-A_0)] = -\kappa_{rev}t$ is used for obtaining the thermodynamic *cis-trans* isomerization rate of AZO, $\kappa_{rev} = 0.166\ h^{-1}$, and $t_{1/2} = \ln2/\kappa_{rev}$ is used for obtaining the half-life of AZO, $t_{1/2} = \ln2/0.166 = 4.18$ h. A_∞ is the absorption intensity of *trans*-AZO rich state after *cis-trans* isomerization. A_t is the absorption intensity of AZO at "t" time. A_0 is the absorption intensity of *cis*-AZO rich state after UV irradiation. Please note: **2** could not under solid-liquid phase change under UV light irradiation. The half-life of solid-state *cis*-**2** is

obtained from a solid sample.

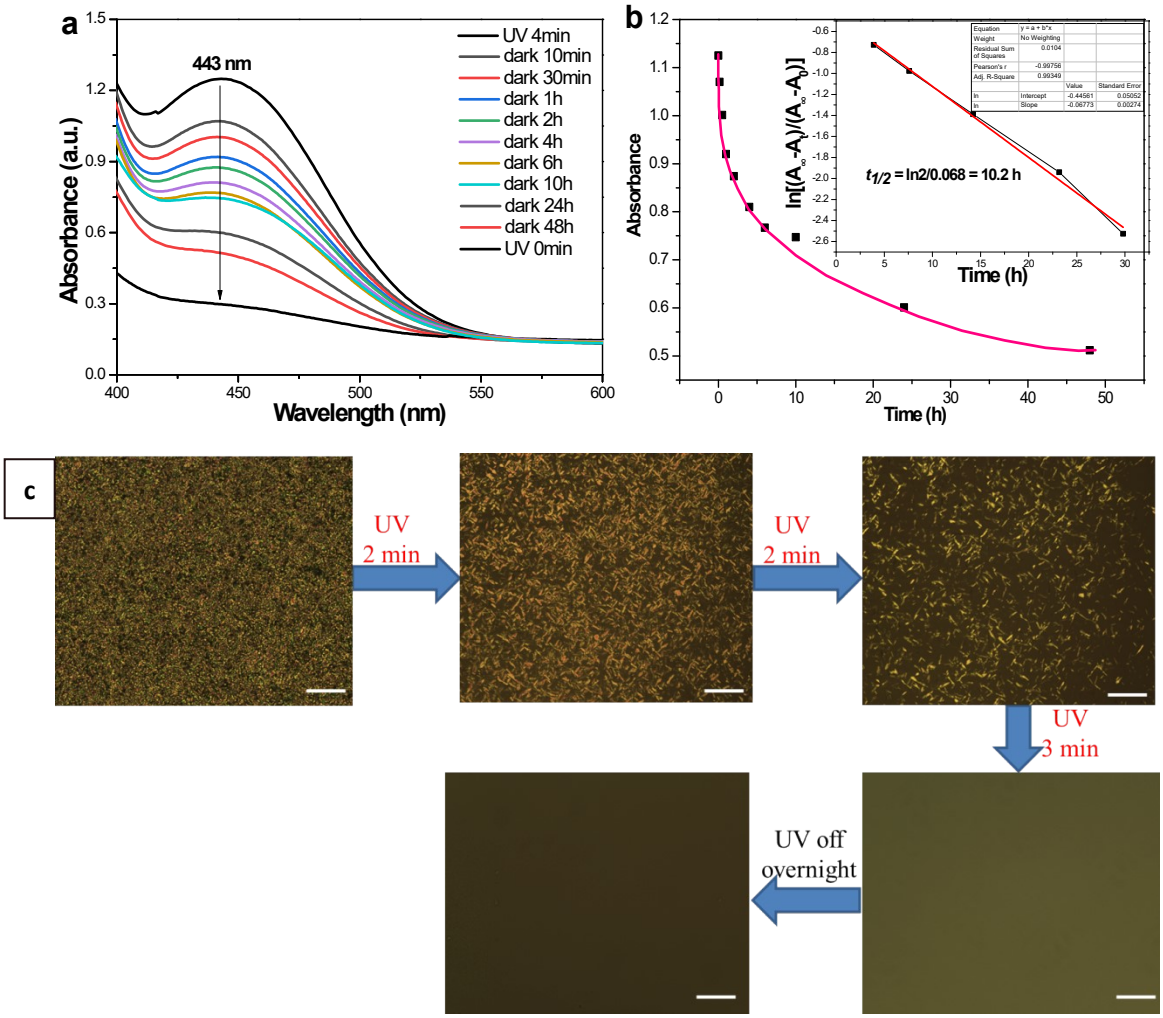

Figure S6. a) Time-dependent UV-Vis absorption spectral changes of pure **1** at r.t. under firstly UV light over 4 min and then in dark. Over 48 h, the absorbance between 400 and 500 nm have not been back to the original state, indicating a slow *cis*→*trans* isomerization process. This slow isomerization process results in a relative stable IL state of pure surfactant **1** at r.t. after ceasing the UV light. b) The absorption peak at 443 nm for π-π* absorption of *cis*-**1** is used for drawing the plotted graph, affording the half-life (10.20 h) for *cis*-**1**, by using a similar calculation method as that in Figure S5d. Please note: the half-life of *cis*-**1** was obtained in liquid state. c) The POM analysis on thermodynamic stability of IL phase of **1** after ceasing UV light at r.t.. Scale bar is 100 μm.

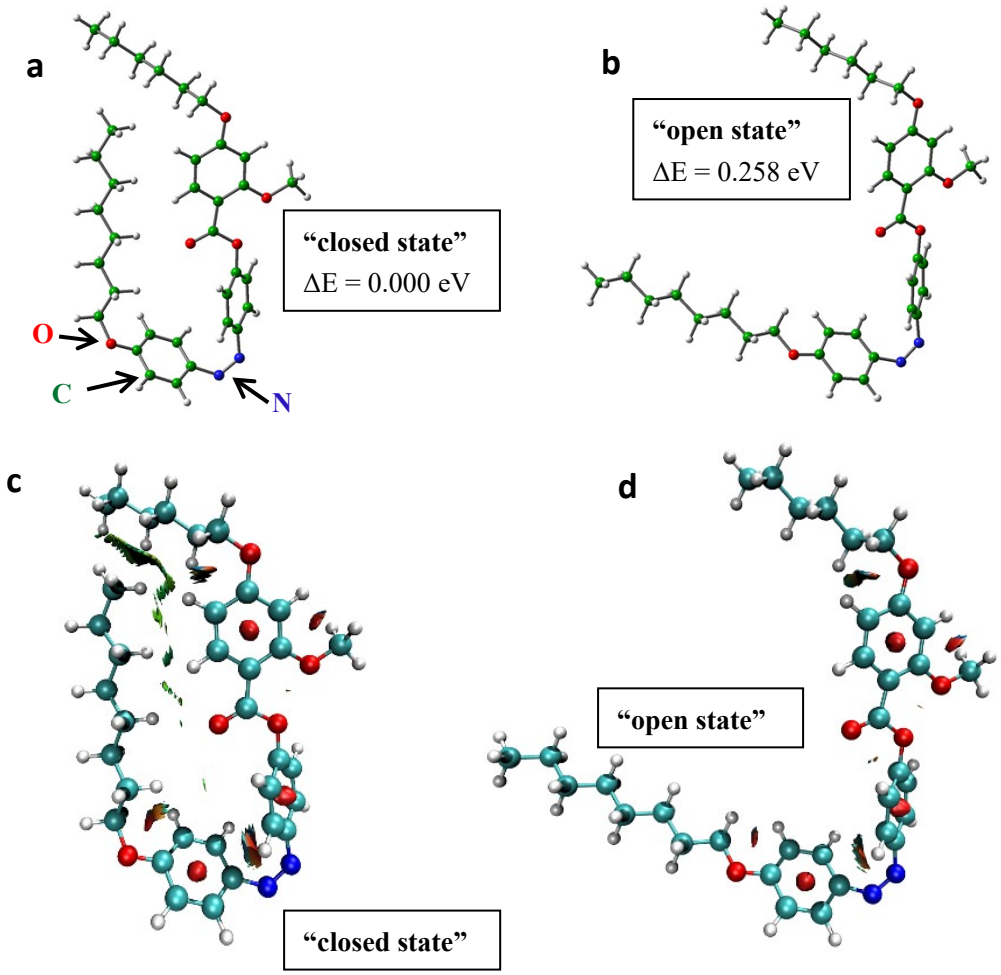

Figure S7. The geometric optimizations of the proposed states of *cis*-**1** were performed within Gaussian 16 program package (Revision D.01)[5] at the level of density functional theory (DFT) B3LYP functional[6] coupled with Grimme D3 dispersion correction[7] and 6-31G (d, p) basis set. To confirm the nature of obtained minima, vibrational frequency calculations were then carried out at the same level of theory as geometric optimizations.

It is conceivable that, the molecules investigated here should have several possible conformations, in particular the alkyl chains of *cis*-**1**. Two possible conformations of *cis*-**1** have been optimized using the hybrid B3LYP functional coupled with the 6-31G (d,p) basis set (see conformation a and b). With the same theory level, frequency analysis was performed to confirm the nature of obtained minima (their structures and relative energies are given) and it is shown that the "closed" conformation from the two alkyl chains is more stable with lower relative energies than the "open" one. This is consistent with our original intention on the design of **1**.

Meanwhile, the visualization of van der Waals interaction between the two alkyl chains can be achieved from the "closed" state through the reduced density gradient (RDG) calculation based on electron density and its derivatives of the corresponding molecule[8-9]. As depicted in c-d, the low-density and low gradient region in "closed" state of *cis*-**1** mainly corresponds to the non-bounded overlaps between alkyl chains, which are originated from van der Waals interactions. The evidently bigger overlapping portion inside the "closed" state than the "open" state further interpret the inherent reason of the relative stability of "closed" state.

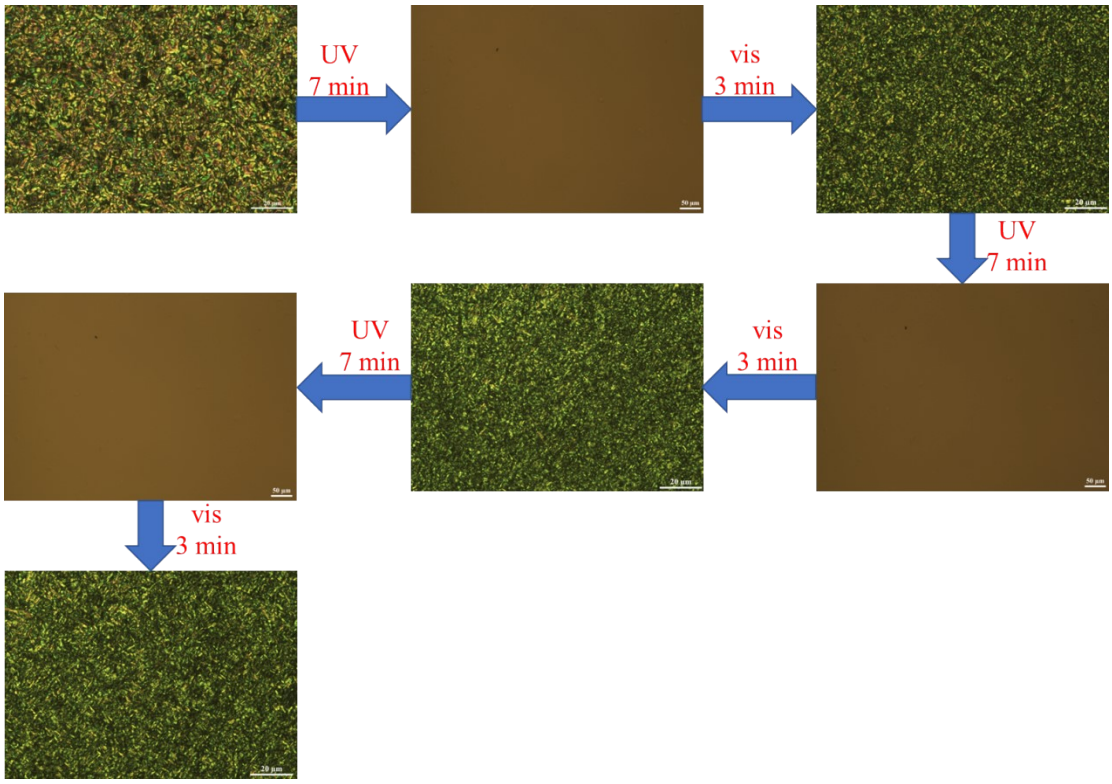

Figure S8. Repeated UV-Vis illuminations induce repeated reversible LC⇄IL phase transitions of **1** at r.t..

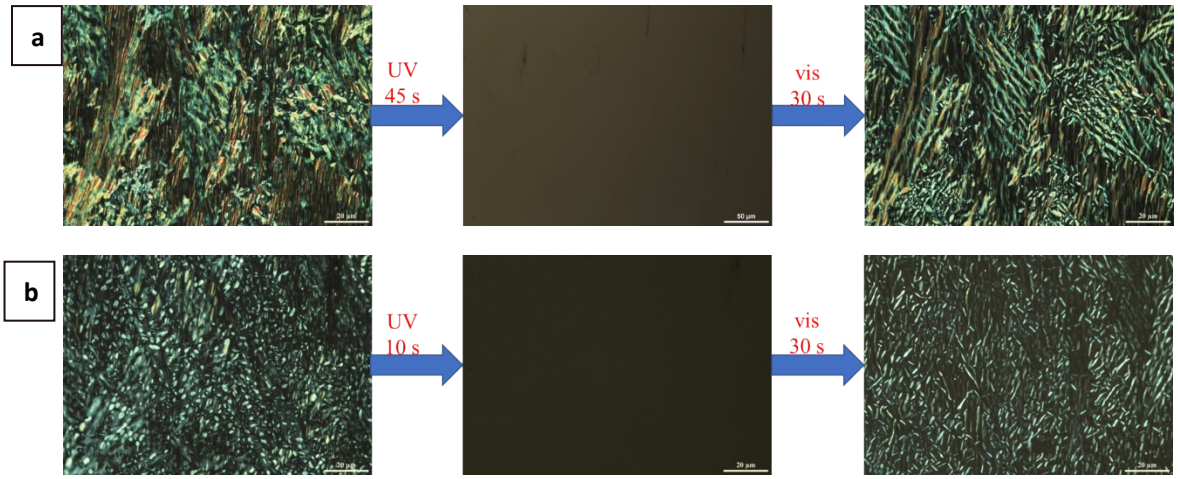

Figure S9. UV-Vis illuminations induce reversible LC⇄IL phase transitions of **1** at a) 40°C and b) 45°C, respectively.

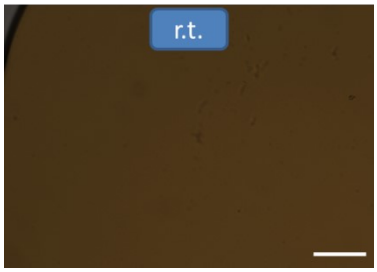

Figure S10. POM images of DNA-**1**-DOAB (1:1:4) at r.t., indicating an isotropic state.

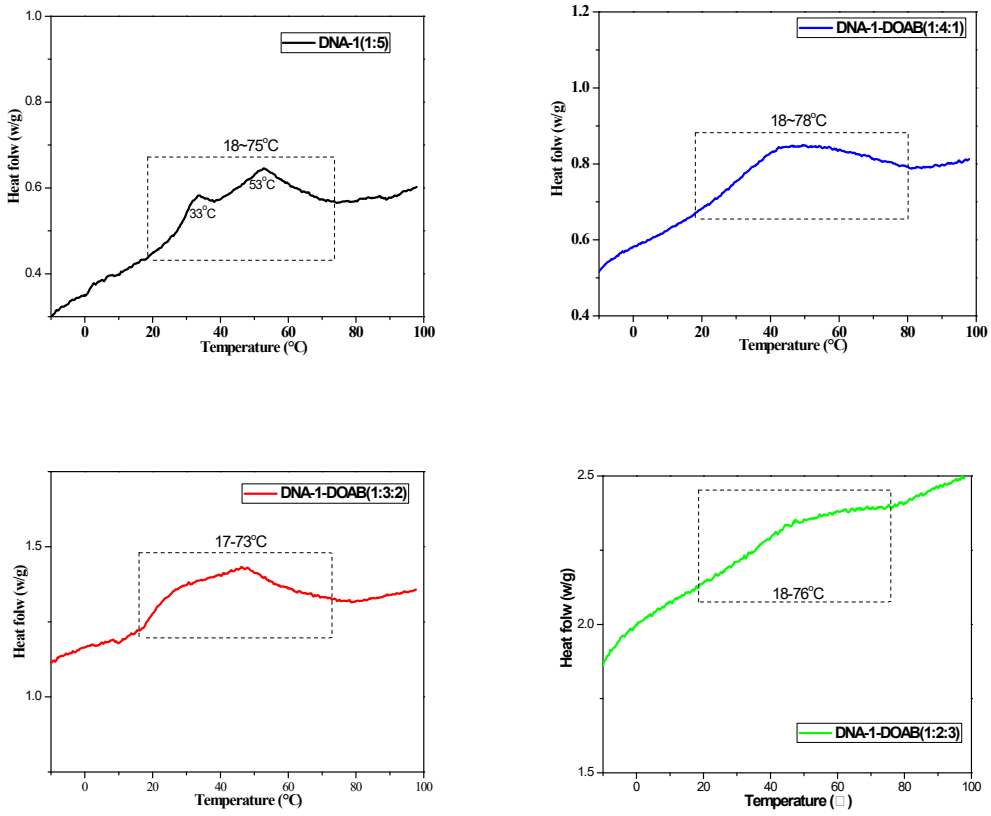

Figure S11. DSC profiles of DNA TLCs. Before the DSC measurements, all the samples were pre-treated by heating to above their clearing points and cooling to r.t. two times.

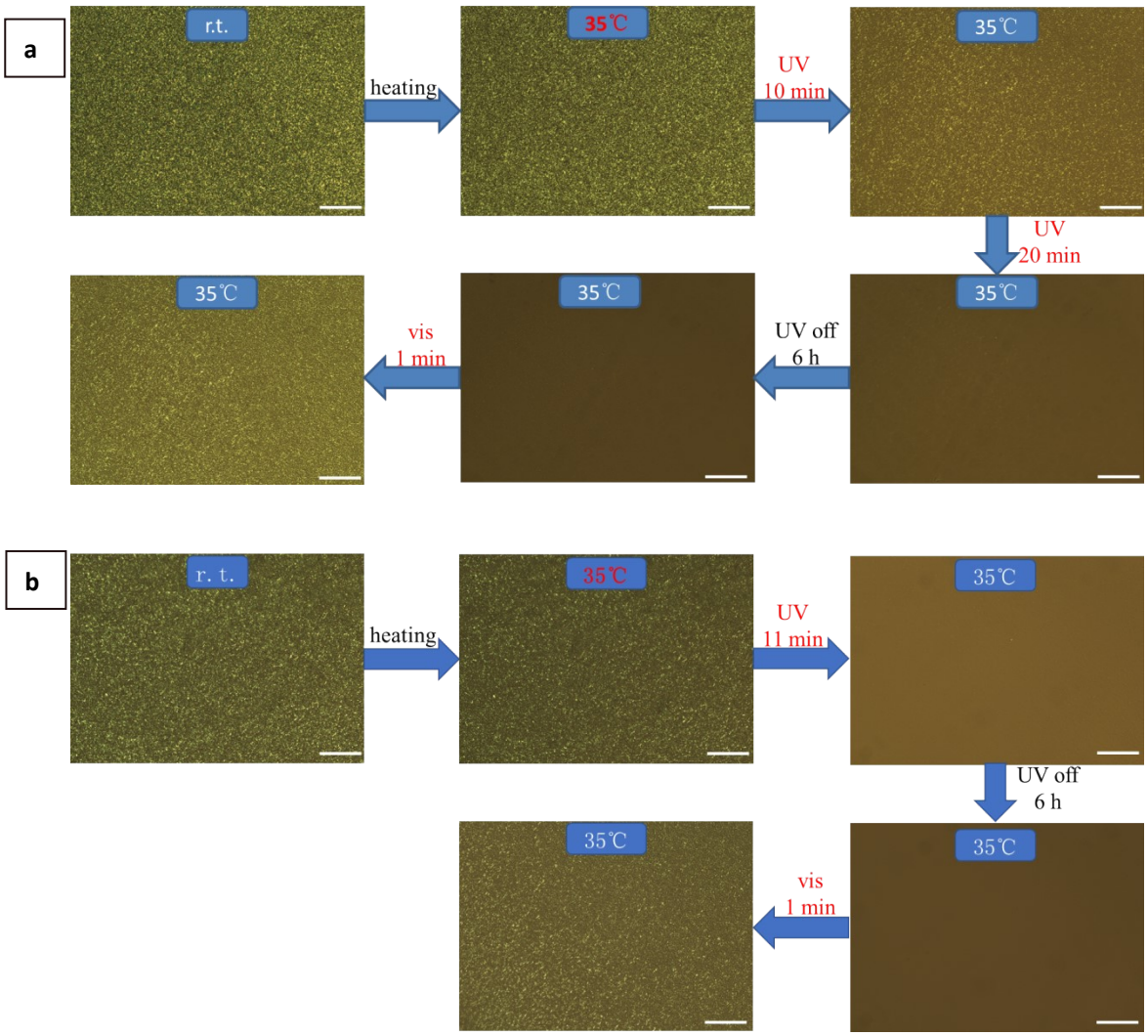

Figure S12. POM images of light-induced phase transitions of a) DNA-**1** (1:5) and b) DNA-**1**-DOAB (1:4:1) at 35 °C. The scale bar is 50 μm.

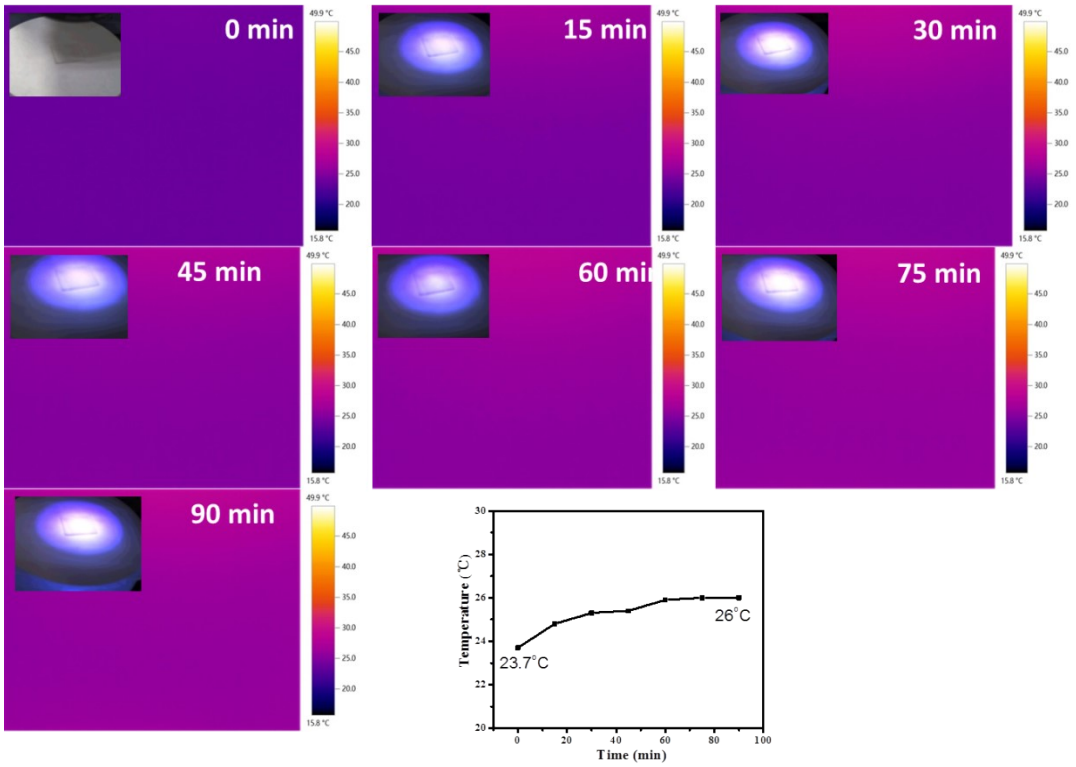

Figure S13. Infrared thermometer images of the testing conditions under irradiation with 365 nm (32 mW cm^{-2}) light over 90 min. The highest surface temperature could only reach to 26 °C.[10]

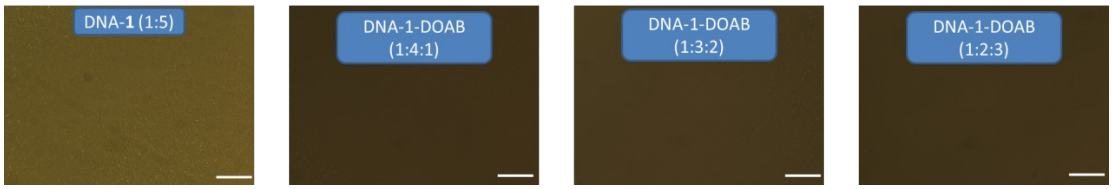

Figure S14. POM images of UV light induced DNA ILs after ceasing UV light at r.t. over 48 h. The scale bar is 50 μm.

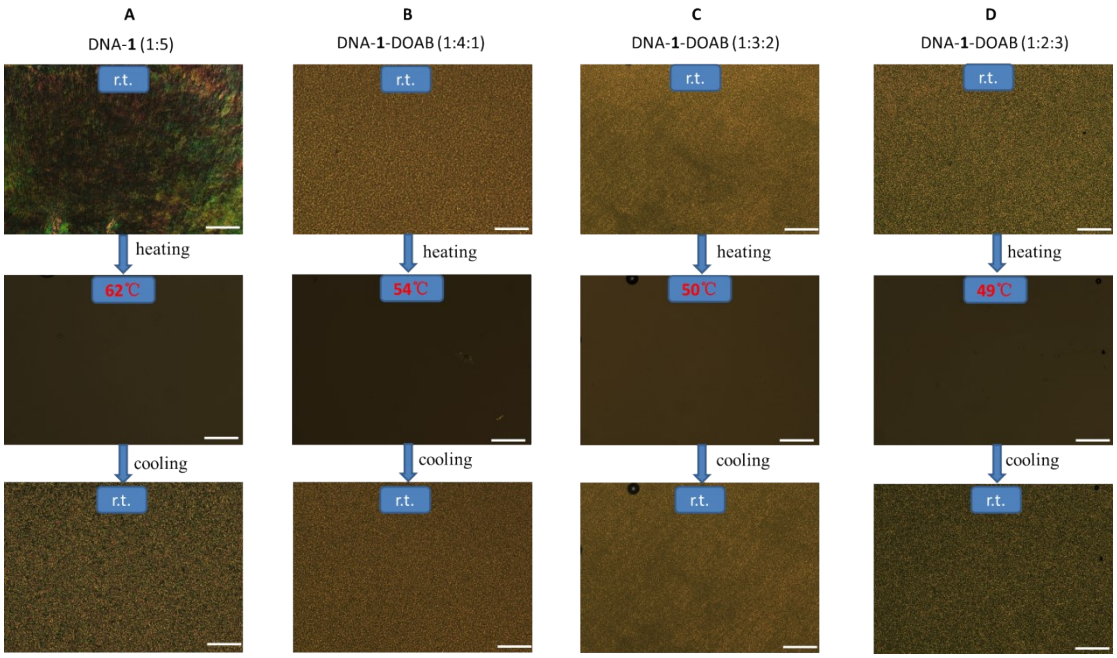

Figure S15. A summary on the temperature-dependent POM analysis of DNA TLCs and DNA IL. The scale bar is 50 μm.

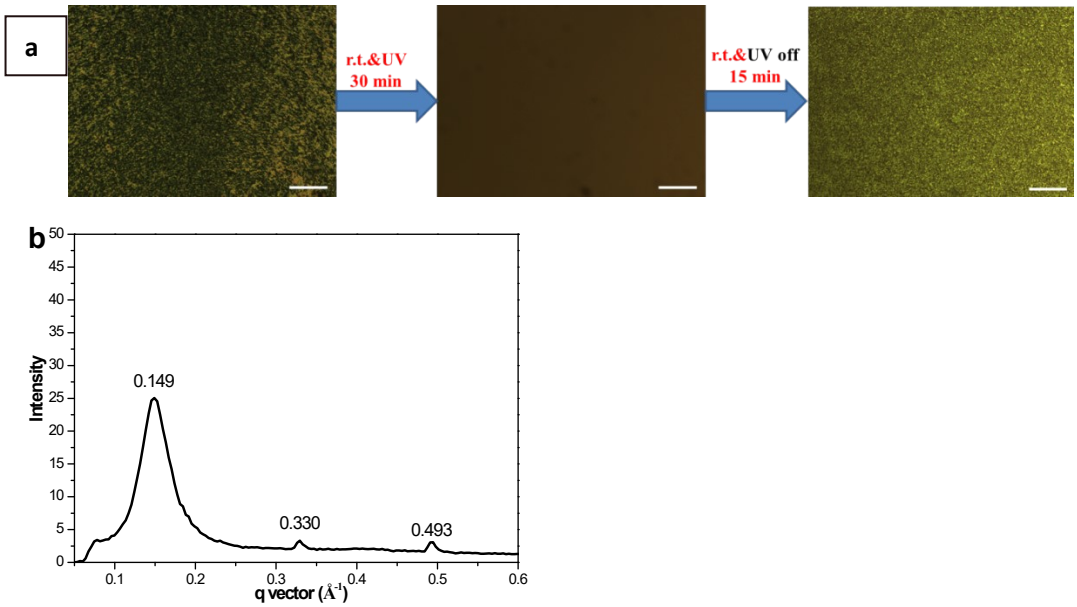

Figure S16. a) POM images of the phase transitions of DNA-**2**-DOAB (1:3:2) under UV light and after ceasing UV light at r.t.. b) The SAXS profile of DNA-**2**-DOAB (1:3:2) at r.t.. Broad diffraction peak at 0.149 $Å^{-1}$ with no following harmonics were observed, indicating the nematic arrangement, which is in accordance with the reported AZO-containing solvent-free biomaterials from the previous studies.[1, 11] The diffraction peaks correspond to the diffraction spacing distances from 4.21 nm, composing of 1.1 nm thickness of DNA[12] and 3.11 nm thickness of surfactants.

Additionally, two peaks at ~0.330 $Å^{-1}$ and ~0.493 $Å^{-1}$ were also observed, while, the ratio between these peaks and the broad diffraction peak at 0.149 $Å^{-1}$ does not correspond to a layered structure or other structures. We attribute them to the harmonic peaks of the first-ordered subsidiary satellite peaks of nematic diffraction peak, indicating an in-plane layer undulation for DNA-**2**-DOAB (1:3:2),[13] of which the first-order subsidiary satellite peak is probably overlapped by the broad diffraction peak.

As compared to **1**, the lack of one alkyl chain in **2** leads to the absence of "locked" *cis*-AZO conformation. As a result, DNA-**2**-DOAB (1:3:2) could not maintain the IL state after ceasing the UV light, transiting back to LC state in short time. The fabrication of DNA-**2**-DOAB (1:3:2) complex was similar to that of DNA-**1** TLCs.

References

1. L. Zhang, S. Maity, K. Liu, Q. Liu, R. Göstl, G. Portale, W. H. Roos and A. Herrmann, *Small*, 2017, **13**, 1701207.
2. L. Zhang, Z. Tang, L. Hou, Y. Qu, Y. Deng, C. Zhang, C. Xie and Z. Wu, *Analyst*, 2020, **145**, 1641-1645.
3. A. K. Saydjari, P. Weis and S. Wu, *Advanced Energy Materials*, 2017, **7**, 1601622.
4. P. Weis, W. Tian and S. Wu, *Chemistry – A European Journal*, 2018, **24**, 6494-6505.
5. M.J. Frisch, G.W. Trucks, H.B. Schlegel, G.E. Scuseria, M.A. Robb, J.R. Cheeseman, G. Scalmani, V. Barone, B. Mennucci, G.A. Petersson, H. Nakatsuji, M. Caricato, X. Li, H.P. Hratchian, A.F. Izmaylov, J. Bloino, G. Zheng, J.L. Sonnenberg, M. Hada, M. Ehara, K. Toyota, R. Fukuda, J. Hasegawa, M. Ishida, T. Nakajima, Y. Honda, O. Kitao, H. Nakai, T. Vreven, J.A. Montgomery, J.E. Peralta, F. Ogliaro, M. Bearpark, J.J. Heyd, E. Brothers, K.N. Kudin, V.N. Staroverov, T. Keith, R. Kobayashi, J. Normand, K. Raghavachari, A. Rendell, J.C. Burant, S.S. Iyengar, J. Tomasi, M. Cossi, N. Rega, M.J. Millam, M. Klene, J.E. Knox, J.B. Cross, V. Bakken, C. Adamo, J. Jaramillo, R. Gomperts, R.E. Stratmann, O. Yazyev, A.J. Austin, R. Cammi, C. Pomelli, J.W. Ochterski, R.L. Martin, K. Morokuma, V.G. Zakrzewski, G.A. Voth, P. Salvador, J.J. Dannenberg, S. Dapprich, A.D. Daniels, Ö. Farkas, J.B. Foresman, J.V. Ortiz, J. Cioslowski, D.J. Fox, 09 Gaussian, Revision D.01, Gaussian, Inc., Wallingford, CT, 2013.
6. A.D. Becke, Journal of Chemical Physics, 1993, 98 (7), 5648-5652.
7. S. Grimme, S. Ehrlich, L. Goerigk, Journal of Computational Chemostry, 2011, 32 (7), 1456-1465.
8. E. R. Johnson, S. Keinan, P. Mori-Sánchez, J. Contreras-García, A. J. Cohen, W. Yang, Journal of the American Chemical Society, 2010, 132, 6498-6506.
9. T. Lu, F. Chen, Journal of Computational Chemostry, 2012, 33 (5), 580-592.
10. L. Zhang, Y. Qu, J. Gu, Z. Tang, Z. Wu and X. Luo, *Acta Biomaterialia*, 2021, **128**, 143-149.
11. L. Zhang, C. Ma, J. Sun, B. Shao, G. Portale, D. Chen, K. Liu and A. Herrmann, *Angew. Chem. Int. Ed.*, 2018, **57**, 6878-6882.

12. T. Neumann, S. Gajria, M. Tirrell and L. Jaeger, *J. Am. Chem. Soc.*, 2009, **131**, 3440-3441.
13. K. Liu, M. Shuai, D. Chen, M. Tuchband, J. Y. Gerasimov, J. Su, Q. Liu, W. Zajaczkowski, W. Pisula, K. Müllen, N. A. Clark and A. Herrmann, *Chemistry – A European Journal*, 2015, **21**, 4898-4903.